




 Cite this: *RSC Adv.*, 2020, 10, 4045

# Enhanced dispersibility of metal–organic frameworks (MOFs) in the organic phase *via* surface modification for TFN nanofiltration membrane preparation†

 Hengrao Liu,<sup>a</sup> Min Zhang,<sup>a</sup> Hao Zhao,<sup>a</sup> Yanjun Jiang,<sup>a</sup> <sup>a</sup> Guanhua Liu <sup>\*ab</sup> and Jing Gao<sup>\*a</sup>

The nanosized UiO-66-NH<sub>2</sub> metal–organic framework (MOF) material was synthesized and modified by palmitoyl chloride to enhance the dispersibility and restrain the aggregation of MOF particles in the organic phase. Then the above nanomaterial was introduced into interfacial polymerization to prepare thin film nanocomposite (TFN) nanofiltration membranes. The prepared membranes displayed “ridge-valley” shaped Turing structure surface morphology with membrane thickness around 380 nm. The FE-SEM, ATR-FTIR and XPS characterization showed the polyamide layer was fabricated on the substrate surface. The TFN membranes showed higher hydrophobicity, zeta potential and roughness than TFC membranes. Due to the introduction of MOF and the formation of MOF/polyamide interfacial passageways, the TFN membranes showed higher water permeability but slightly lower rejection properties than TFC membranes. Compared with the TFN membranes prepared from pristine UiO-66 and UiO-66-NH<sub>2</sub>, the TFN membrane prepared from modified UiO-66-NH<sub>2</sub> showed better rejection properties because of its superior dispersibility in the organic phase.

 Received 19th November 2019  
 Accepted 12th January 2020

DOI: 10.1039/c9ra09672h

[rsc.li/rsc-advances](http://rsc.li/rsc-advances)

## 1 Introduction

Separation is one of the most crucial processes in the chemical industry. Conventional separation technologies, such as distillation, adsorption, and extraction, consume vast amounts of energy or chemical materials. So developing an energy-saving and economical separation technology is of great significance in the chemical industry. Membrane separation is a promising candidate that has emerged in recent decades by reason of no phase transition, energy-efficiency, simple equipment requirement and easy operation process.<sup>1–3</sup>

Nanofiltration is a kind of membrane separation technology, possessing a membrane pore size about 1 nm.<sup>4</sup> Polyamide (PA) thin film composite (TFC) membrane was widely used in nanofiltration and reverse osmosis such as desalination, dye separation and waste water treatment, but the “trade-off” effect between permeability and selectivity is a common problem in TFC membrane.<sup>5</sup> Researchers have made great effort to improve the permeability of TFC membrane without losing solute selectivity. Hoek and his coworkers brought forward the idea of

fabricating thin film nanocomposite (TFN) membranes by incorporating zeolite nanoparticles within the polyamide matrix.<sup>6</sup> In their research, the TFN membranes showed increased permeability with the increase of filler loading and still maintained high rejection property. From then on, many kinds of inorganic nanomaterials (such as SiO<sub>2</sub>, TiO<sub>2</sub>, graphene oxide and carbon nanotube) were introduced into interfacial polymerization process to prepare TFN membranes.<sup>7</sup> The incorporated nanomaterials could create additional passageways for solvent transfer through their interconnected nanopores or nanomaterial–polyamide interfaces.

Metal–organic frameworks (MOFs) are a series of porous organic–inorganic hybrid materials, which consist of inorganic metal nodes linked with organic ligands by coordination bonds.<sup>8</sup> The intrinsic nanopores of MOFs can be employed as the solvent transfer passageways in nanofiltration process.<sup>9</sup> Furthermore, the size of particle/pore, and the property of surface/pore are highly tunable to meet the demand of membrane preparation.<sup>10</sup> In addition, the presence of organic ligands results in better compatibility with polymer matrix. So MOFs are regarded as ideal materials to prepare TFN membranes. In traditional ways, if MOFs are dispersed in aqueous phase in interfacial polymerization process to prepare TFN membrane, a large amount of MOFs will be removed together with the excess amine solution, leaving only very little MOFs loaded on the substrate surface, which restricts the effect

<sup>a</sup>School of Chemical Engineering and Technology, Hebei University of Technology, Tianjin 300130, China. E-mail: ghliu@hebut.edu.cn; jgao@hebut.edu.cn

<sup>b</sup>Tianjin Key Laboratory of Chemical Process Safety, Hebei University of Technology, Tianjin 300130, China

† Electronic supplementary information (ESI) available. See DOI: 10.1039/c9ra09672h



of the MOFs.<sup>11</sup> While one of the greatest challenge to disperse MOF nanoparticles in organic phase is the particle aggregation,<sup>12</sup> which is ascribed to the poor dispersibility of nanomaterials in membrane casting solution especially in organic phase. The aggregation tendency of inorganic nanoparticles in solution was an intrinsic challenge because of the high surface energy, large specific surface area and strong interaction between nanoparticles. Under these factors, nanoparticles are easy to aggregate together to reduce the total surface energy of particles which eventually reaches an equilibrium state. The serious aggregation of nanoparticles may bring defects into TFN membrane's selective layer, which can lead to significant decrease of rejection property. To restrain the aggregation of MOF nanoparticles, Li *et al.* prepared high-performance MOF based nanofiltration membranes by coordination-driven *in situ* self-assembly method,<sup>13,14</sup> the prepared membranes showed outstanding nanofiltration performance. Zhu *et al.* modified ZIF-8 MOF particles with poly(sodium 4-styrenesulfonate) and introduced it into interfacial polymerization.<sup>15</sup> The prepared TFN nanofiltration membrane showed obvious increase in water permeability and achieved analogous rejection property at low ZIF-8 loading amount. Guo *et al.* synthesized UiO-66-NH<sub>2</sub> and modified the surface by dodecyl aldehyde to prepare TFN membranes for organic solvent nanofiltration.<sup>16</sup> The TFN membrane exhibited both high methanol permeance and high rejection to tetracycline. From the above instances, surface modification is a promising method to improve dispersibility and reduce aggregation of nanoparticles in the preparation process of TFN membranes.

Among various MOFs, zirconium MOFs aroused great concern of researchers due to the high stability, diverse organic ligands with changeable function groups (for example -NH<sub>2</sub>, -OH, -COOH and so on),<sup>17,18</sup> and ease of modification to change the surface property. UiO-66-NH<sub>2</sub> was a kind of Zr-based MOFs, which was made up of Zr ions linked by 2-aminobenzene-1,4-dicarboxylic acid organic ligands. The highly reactive -NH<sub>2</sub> groups situated in the internal pores and outside surface of UiO-66-NH<sub>2</sub>, which made it possible to be easily modified by various chemical reagents to change its surface property and increase the dispersity in casting solution.

For this reason, UiO-66-NH<sub>2</sub> nanomaterial was synthesized and the outside surface was modified by palmitoyl chloride in a facile way, then the modified UiO-66-NH<sub>2</sub> nanomaterial was dispersed in TMC/cyclohexane organic phase and introduced into interfacial polymerization process to fabricate TFN membranes. On the one hand, the long alkyl chain of palmitoyl chloride on the outside surface can increase the compatibility between UiO-66-NH<sub>2</sub> nanoparticles and nonpolar organic solvent because of their similar polarity, and hence decrease the aggregation tendency between nanoparticles. On the other hand, compared with *n*-hexane used in most researches, the use of cyclohexane as organic solvent in this study can lead to better dispersity of nanomaterial in organic phase. For the above-mentioned reasons, the modified UiO-66-NH<sub>2</sub> nanoparticles can get good dispersibility in organic phase to form stable suspension of nanoparticles during interfacial polymerization to inhabit the formation of nonselective defects in TFN

membranes. The morphology, ATR-FTIR, XPS, hydrophilicity, zeta potential, and surface roughness of the prepared membranes were characterized. The influence of the modified UiO-66-NH<sub>2</sub>-PC concentration in organic phase on membrane property and the long-term stability of the membrane was investigated in detail.

## 2 Experimental section

### 2.1 Materials and reagents

Commercial polyacrylonitrile (PAN) ultrafiltration membrane (MWCO: 50 000) was bought from Beijing Separate Equipment Co. Ltd. NaOH, Na<sub>2</sub>SO<sub>4</sub>, MgSO<sub>4</sub>, NaCl, *n*-hexane, cyclohexane, trichloromethane (CHCl<sub>3</sub>), triethylamine, and acetic acid glacial were bought from Tianjin Fengchuan Chemical Reagent Technologies Co. Ltd. Zirconium chloride (ZrCl<sub>4</sub>), piperazine (PIP), *N,N*-dimethylformamide (DMF), and benzene-1,3,5-tricarbonyl trichloride (TMC) were bought from Aladdin Biochemical Technology Co. Ltd. Palmitoyl chloride was bought from Macklin Biochemical Co. Ltd. 2-Aminoterephthalic acid (NH<sub>2</sub>-BDC) was bought from Dibai Chemical Technology Co. Ltd.

### 2.2 Synthesis and modification of UiO-66-NH<sub>2</sub> nanomaterial

Zr-based MOFs UiO-66-NH<sub>2</sub> nanomaterial was synthesized as follows: ZrCl<sub>4</sub> (0.686 mmol) and NH<sub>2</sub>-BDC (0.686 mmol) were dissolved in 40 mL DMF. Then 20 μL H<sub>2</sub>O and 1.2 mL acetic acid glacial were added. Acetic acid glacial could decrease growth rate of Zr-based MOF crystals and hence increase the crystallinity of MOF nanoparticles. The OH<sup>-</sup> of water molecules could be employed as the composition of secondary building units in UiO-66-NH<sub>2</sub> crystal structure. The above mixture was sonicated and stirred to dissolve completely and then heated at 100 °C for 24 h. The resulting product was centrifuged and washed 3 times by DMF and then washed 2 times by ethanol. 1 mL UiO-66-NH<sub>2</sub> suspension was dried thoroughly to confirm the weight and concentration of UiO-66-NH<sub>2</sub>.

The above purified UiO-66-NH<sub>2</sub> nanoparticles (2 g) were dispersed in the mixture of 40 mL CHCl<sub>3</sub> and 2.4 mL palmitoyl chloride. 1.4 mL triethylamine was added afterwards. The resultant mixture was sonicated to disperse and stirred at room temperature overnight to make UiO-66-NH<sub>2</sub> react with palmitoyl chloride. The product was washed by CHCl<sub>3</sub> 3 times and cyclohexane 3 times and then re-dispersed in cyclohexane. The modified UiO-66-NH<sub>2</sub> was named as UiO-66-NH<sub>2</sub>-PC. The modification scheme was displayed in Fig. S1† and the method of calibrating UiO-66-NH<sub>2</sub>-PC concentration was similar to that of UiO-66-NH<sub>2</sub>.

### 2.3 Hydrolyzation of PAN substrate membrane

The commercially available PAN ultrafiltration membrane was used as the substrate to prepare nanofiltration membranes. Prior to the preparation process, the PAN ultrafiltration membrane was put in NaOH solution (1 mol L<sup>-1</sup>) at 50 °C for 1 h to make -CN hydrolyze to -COOH, and the resultant membrane was denoted as HPAN. The existence of ionized -COOH can adsorb electropositive amine monomer in the following



interfacial polymerization process and increase the hydrophilicity of the substrate.

#### 2.4 Preparation of TFC and TFN membranes

The TFN membranes were prepared by interfacial polymerization. Before the preparation process, the UiO-66-NH<sub>2</sub>-PC nanoparticles with different concentration (0.05% w/v, 0.10% w/v, and 0.15% w/v) were dispersed into TMC/cyclohexane organic solution (0.15% w/v). The HPAN substrate membrane was immersed in PIP aqueous solution (0.15% w/v) for 20 min. Then the substrate was taken out from PIP solution and removed the excess solution on the substrate surface by dustless bibulous paper. Afterwards, the substrate membrane with PIP solution inside the pores was immersed into the above organic solution for 2 min. The membranes prepared with the UiO-66-NH<sub>2</sub>-PC concentration of 0.05% w/v, 0.10% w/v, and 0.15% w/v in organic solution were named as TFN-0.05, TFN-0.10 and TFN-0.15, respectively. The concentration of UiO-66-NH<sub>2</sub>-PC in organic solution could be confirmed by different volume of UiO-66-NH<sub>2</sub>-PC suspension. The schematic diagram was shown in Fig. 1.

The TFC membrane was prepared by the similar method of TFN membranes without adding UiO-66-NH<sub>2</sub>-PC nanoparticles in organic phase.

#### 2.5 Characterization methods

Field emission scanning electron microscopy (FE-SEM FEI Nova NanoSEM450) was employed to observe the morphologies of UiO-66-NH<sub>2</sub> and UiO-66-NH<sub>2</sub>-PC. The surface and cross-section morphologies of TFC and TFN membranes were also observed by FE-SEM. Fourier transform infrared (FTIR) spectra were obtained through a Bruker Vertex 70 spectrometer to characterize the chemical constitutions of UiO-66-NH<sub>2</sub>, UiO-66-NH<sub>2</sub>-PC and

the prepared membranes. Water contact angles of TFC and TFN membranes were measured by an optical contact angle measuring system (KRUSS DSA-100). The crystallinities of synthesized UiO-66-NH<sub>2</sub> and UiO-66-NH<sub>2</sub>-PC were confirmed by the X-ray diffractometer (XRD, Bruker AXS D8 Focus). Zeta potential of the prepared membranes was tested by SurPASS electrokinetic analyzer (Anton Paar GmbH), and the roughness was measured by Atomic Force Microscope (AFM, Bruker).

#### 2.6 Measurement of nanofiltration performance

The permeability and rejection properties of the membranes were measured using a dead-end filtration equipment with magnetic stirring function to evaluate the nanofiltration performance. Before measurement, the as-prepared membranes was cut into a rotundity with specific diameter and then the membrane was placed into a filtration cell. The membranes was pre-filtrated at 4 bar for 50 min to reach a stable condition. Then the pure water permeability (PWP) and rejection properties were measured with the duration of 3 min.

PWP could be calculated as follows:

$$J = \frac{V}{A \times t \times \Delta P}$$

where  $V$  (L) represents the volume of pure water passing through the membrane;  $A$  (m<sup>2</sup>) is the effective area of the measured membranes;  $t$  (h) is the filtration time and  $\Delta P$  (bar) is the operation pressure. The unit of  $J$  is L (m<sup>-2</sup> h<sup>-1</sup> bar<sup>-1</sup>) or LMH bar<sup>-1</sup>.

Rejection properties were measured by divalent and monovalent salt solution (MgSO<sub>4</sub>, Na<sub>2</sub>SO<sub>4</sub> and NaCl, 0.1% w/v), the rejection for each salt solution could be determined as follows:

$$R(\%) = 1 - \frac{C_p}{C_f}$$

where  $C_p$  is the salt concentrations at permeate side and  $C_f$  is the concentration at feed side. The conductivity of each salt solution could be measured by a conductivity meter. The salt concentration was calculated by solution conductivity and standard curves plotted in advance.

## 3 Results and discussion

### 3.1 Characterization of UiO-66-NH<sub>2</sub> and UiO-66-NH<sub>2</sub>-PC

The morphologies of the synthesized UiO-66-NH<sub>2</sub> and UiO-66-NH<sub>2</sub>-PC were shown in Fig. 2. The regular-octahedral appearance could be clearly seen in the figures. The particle size of UiO-66-NH<sub>2</sub> was about 80–90 nm. After modification, the particles size enlarged a little to about 100 nm.

To further characterize the well-synthesized UiO-66-NH<sub>2</sub> nanoparticles, the XRD patterns were applied to analyze the structure of synthesized material. In Fig. 3, the measured diffraction pattern of UiO-66-NH<sub>2</sub> was in consistent with the reported literature,<sup>12,19</sup> which confirmed the great crystallinity of the synthesized UiO-66-NH<sub>2</sub>. The sharp characteristic peaks at  $2\theta = 7.3^\circ$ ,  $8.4^\circ$  and  $25.7^\circ$  were ascribed to (1 1 1), (2 0 0) and (6 0 0) crystal planes, respectively. After modified by palmitoyl chloride, the XRD pattern of UiO-66-NH<sub>2</sub>-PC remained



Fig. 1 Schematic diagram of the preparation process of TFN membranes.





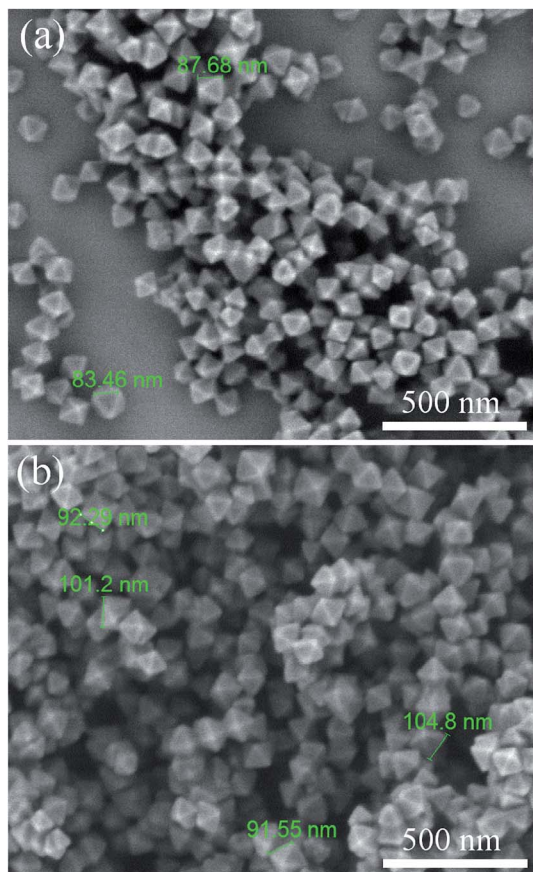


Fig. 2 FE-SEM images of (a) UiO-66-NH<sub>2</sub> and (b) UiO-66-NH<sub>2</sub>-PC.

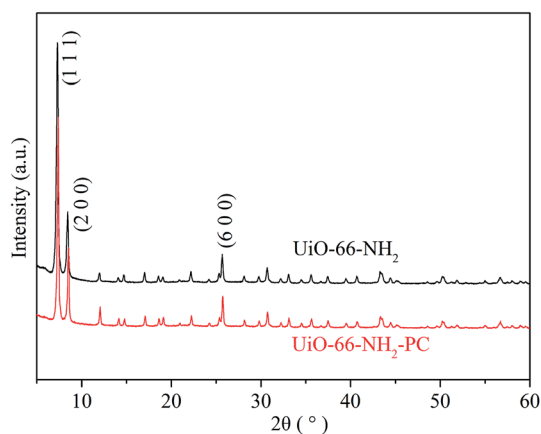


Fig. 3 XRD patterns of UiO-66-NH<sub>2</sub> and UiO-66-NH<sub>2</sub>-PC.

unchanged, indicating the crystal structure was maintained. The regular-octahedral morphology, nanosized particles and the accurate XRD pattern revealed the successful synthesis of UiO-66-NH<sub>2</sub> nanoparticles.

Fig. 4 shows the FT-IR spectra of the synthesized UiO-66-NH<sub>2</sub> and UiO-66-NH<sub>2</sub>-PC. The absorption band at about 3200–3600 cm<sup>-1</sup> was ascribed to the stretching vibration of –NH<sub>2</sub>. The absorption peaks at 1574 and 1257 cm<sup>-1</sup> were ascribed to the

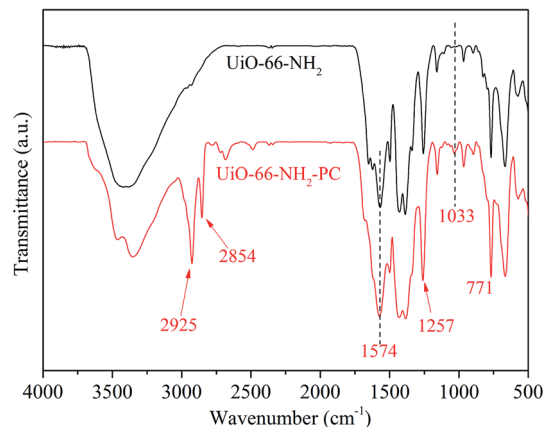


Fig. 4 FT-IR spectra of UiO-66-NH<sub>2</sub> and UiO-66-NH<sub>2</sub>-PC.

stretching vibration of C–O and C–N in NH<sub>2</sub>-BDC, respectively. The absorption peak at 771 cm<sup>-1</sup> was ascribed to the Zr–O bonds of metal nodes in the framework.<sup>12</sup>

The new absorption peaks at 2925 and 2854 cm<sup>-1</sup>, which were appeared only in UiO-66-NH<sub>2</sub>-PC, were ascribed to C–H stretching vibration of the modified palmitoyl chloride. And the new absorption peak at 1033 cm<sup>-1</sup> was ascribed to C–C stretching vibration of palmitoyl chloride.<sup>16</sup> These 3 new absorption peaks indicated that the surface of UiO-66-NH<sub>2</sub> was successfully modified by palmitoyl chloride.

The dispersibility of nanoparticles in solvent depends on the interaction within particles, and the interaction between particle and solvent. The surface modification of UiO-66-NH<sub>2</sub> by palmitoyl chloride could increase the compatibility between particle and solvent, which enhanced the dispersibility in nonpolar solvent (such as *n*-hexane and cyclohexane). In order to confirm the above assumption, UiO-66-NH<sub>2</sub> and UiO-66-NH<sub>2</sub>-PC nanoparticles were dispersed in *n*-hexane and cyclohexane by ultrasonication and then stood for specific time. The unmodified UiO-66-NH<sub>2</sub> particles precipitated immediately in few seconds in *n*-hexane indicating the strong interaction between particles in *n*-hexane, which was in consistent with the phenomenon of other researchers.<sup>16</sup> This phenomenon revealed that it's impossible to disperse UiO-66-NH<sub>2</sub> in *n*-hexane. Fig. 5 showed the dispersibility of UiO-66-NH<sub>2</sub> and UiO-66-NH<sub>2</sub>-PC in *n*-hexane and cyclohexane. After still standing for 30 min, the unmodified UiO-66-NH<sub>2</sub> particles precipitated completely in cyclohexane, and the UiO-66-NH<sub>2</sub>-PC particles began to precipitate in *n*-hexane, but the UiO-66-NH<sub>2</sub>-PC particles still well suspended in cyclohexane. After still standing for 12 h, only UiO-66-NH<sub>2</sub>-PC particles could suspend in cyclohexane. The dispersibility experiment indicated that cyclohexane (rather than *n*-hexane) was better for the nanoparticle dispersion in this study, and surface modification of UiO-66-NH<sub>2</sub> by palmitoyl chloride could significantly increase the dispersibility of the synthesized nanoparticles in nonpolar organic solvent. It could be deduced reasonably that the use of cyclohexane as organic solvent and surface modification of nanoparticles could lead to the best dispersion state of UiO-66-NH<sub>2</sub> in organic phase during



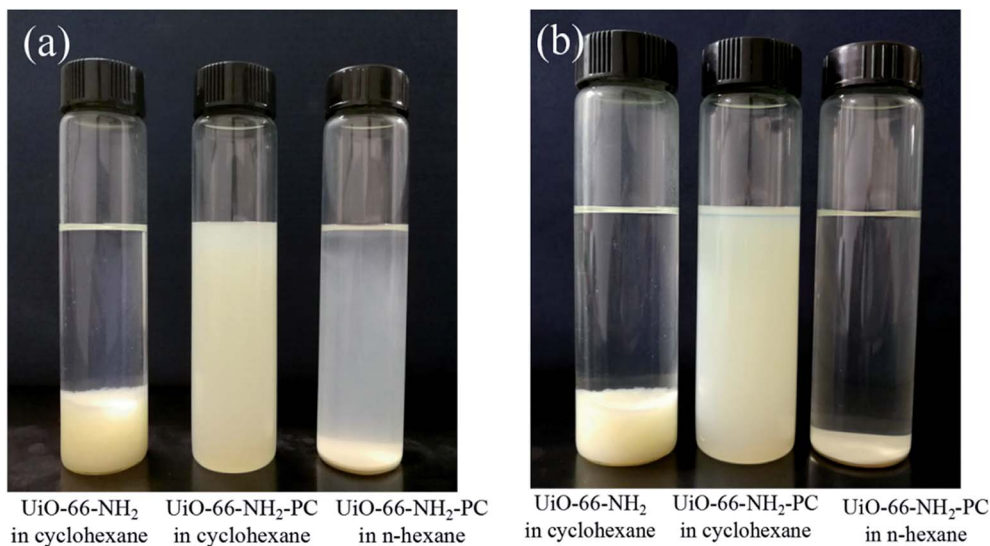


Fig. 5 Dispersibility of UiO-66-NH<sub>2</sub> and UiO-66-NH<sub>2</sub>-PC in cyclohexane and *n*-hexane after standing for (a) 30 min and (b) 12 h.

the preparation process of TFN membranes by interfacial polymerization.

### 3.2 Characterization of the prepared membranes

**3.2.1 Morphologies of TFC and TFN membranes.** The surface morphologies of TFC and TFN membranes were observed by FE-SEM, and the SEM images were shown in Fig. 6.

The prepared TFC membrane showed typical “ridge-valley” morphology. The white and bright stripe was the convex ridge, and the dark background was the valley region. This striped

morphology was a kind of Turing structure, which was different from the spotted morphology in other literature.<sup>20–22</sup> The morphology of nanofiltration membranes prepared by interfacial polymerization depended on many factors: the property of the substrate, the diffusion rate of PIP at water/organic interface, and the interaction between amine monomer and the substrate, *etc.* Generally, the initial interfacial polymerization proceeds at water/organic interface and the PA selective layer grows towards the organic phase side along with the PIP monomers diffusing from water to organic phase because of

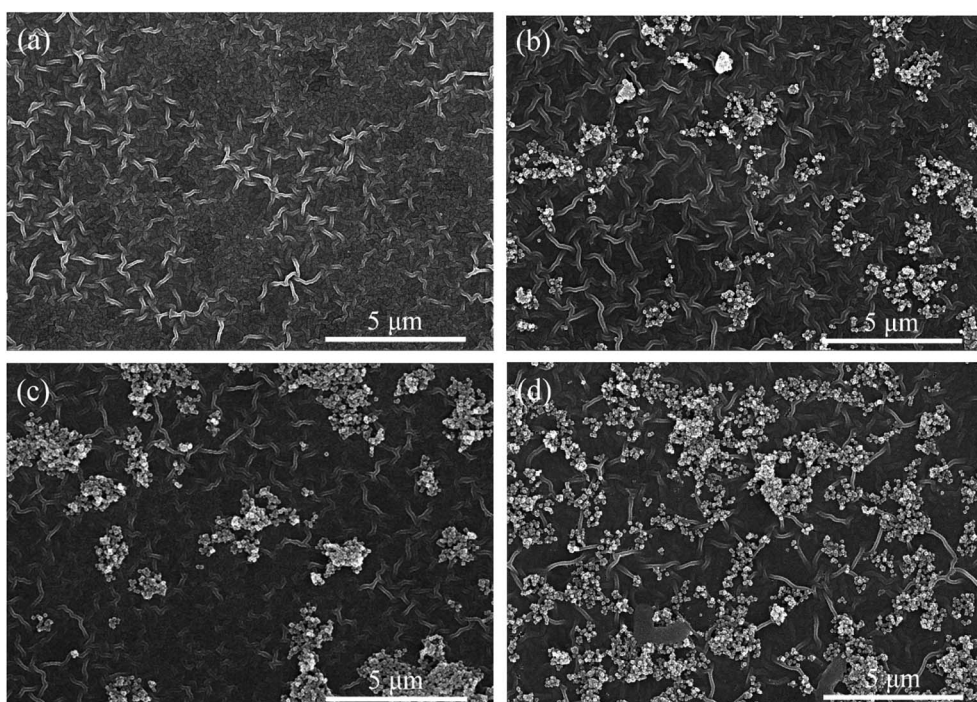


Fig. 6 FE-SEM images of surface morphologies of TFC (a), TFN-0.05 (b), TFN-0.10 (c), TFN-0.15 (d) membranes.





the disadvantageous partition coefficient of the acid chloride monomers in water. The diffusion rate of the two monomers has a remarkable impact on the morphology of TFC membranes. Under most conditions, the diffusion rate of PIP is less than that of TMC, but the diffusion rate disparity of the two monomers is not very significant (within the same order of magnitude), which leads to spotted morphology in the polyamide membrane. When the diffusion rate disparity of the two monomers comes up to orders of magnitude leading to diffusion-driven instability, the striped Turing structure could appear.<sup>23</sup> In this study, the HPAN substrate contained abundant negative charged carboxyl groups that could interact with PIP monomers *via* electrostatic force and hydrogen bonds, which decreased the diffusion rate of PIP molecules during the interfacial polymerization process. So in this study, the diffusion rate of PIP was much lower than that of TMC molecules, which resulted in the striped Turing structure morphology of the TFC membrane in Fig. 6(a). However, the morphology of TFC membrane in another literature was different,<sup>15</sup> which might be ascribed to the different hydrolytic degree of PAN substrate.

As shown in Fig. 6(b–d), the surfaces of TFN membrane also displayed the striped Turing structure morphology with UiO-66-NH<sub>2</sub>-PC loading on the membrane surfaces. The UiO-66-NH<sub>2</sub>-PC nanoparticles distributed more densely on membrane surfaces with the increase of UiO-66-NH<sub>2</sub>-PC concentration in organic phase.

The cross-section morphologies of the prepared membranes were shown in Fig. 7. Compared with HPAN substrate, the prepared nanofiltration membranes presented porous substrate with PA selective layer tightly covering on the top surface. And no interfacial defects between the selective layer and support layer could be found, which could be attributed to the electrostatic interaction between the substrate and PIP indicating the good interfacial compatibility. The thickness of the PA selective layer for each membrane was around 380 nm, which was marked by the red parallel lines in the images.

**3.2.2 Chemical characterization of the prepared membranes.** The ATR-FTIR spectra of the prepared membranes were presented in Fig. 8. The absorption band from 3200 to 3600 cm<sup>-1</sup> was ascribed to the stretching vibration of unreacted amino groups of PIP monomer.<sup>24</sup> The absorption peak at

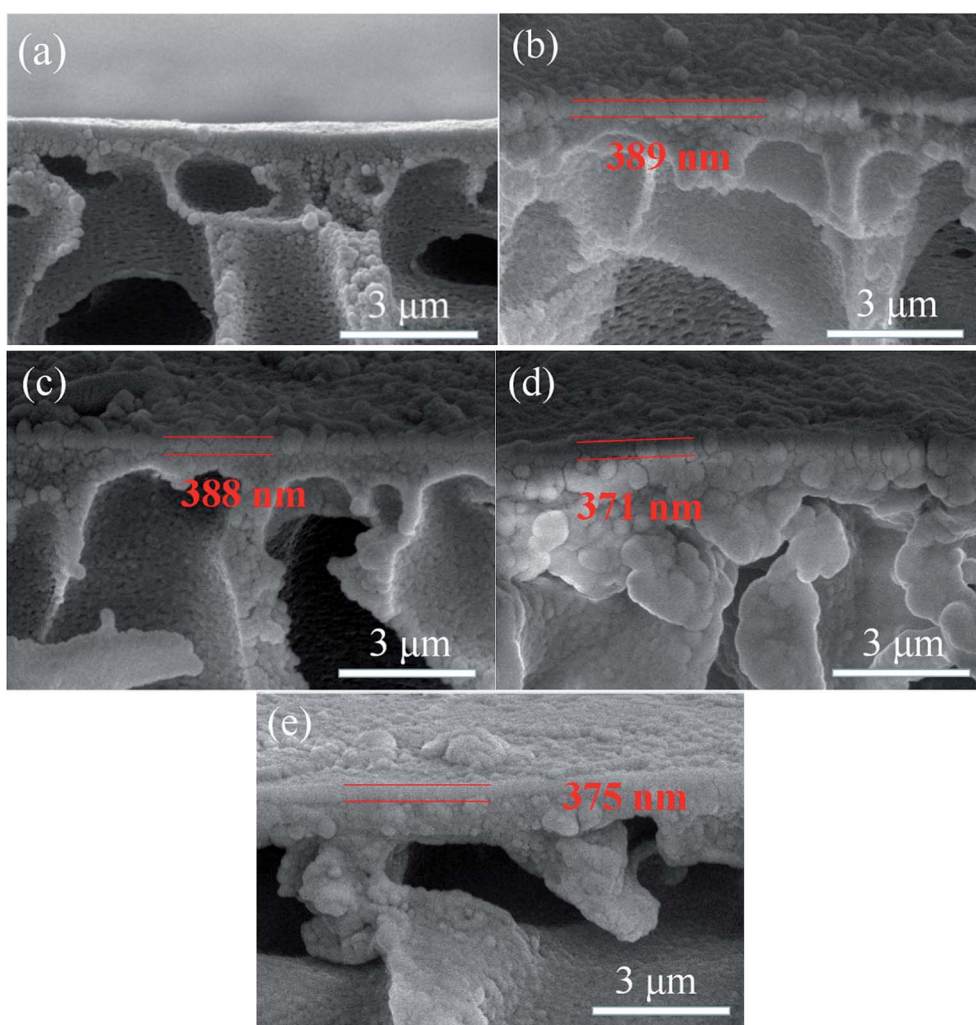


Fig. 7 FE-SEM images of cross-section morphologies of HPAN substrate (a), TFC (b), TFN-0.05 (c), TFN-0.10 (d), TFN-0.15 (e) membranes.



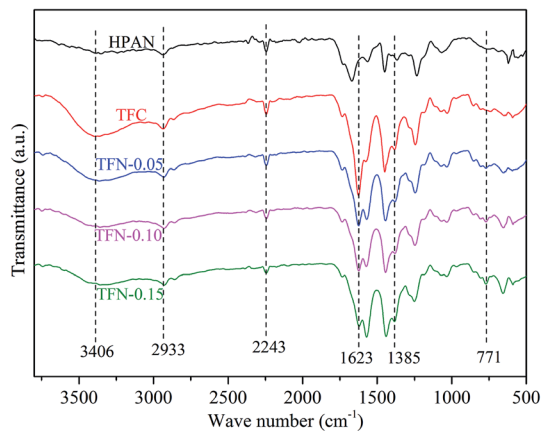


Fig. 8 ATR-FTIR spectra of the prepared membranes.

2933  $\text{cm}^{-1}$  appeared in all membranes, which was related to the stretching vibration of  $-\text{OH}$  in carboxyl groups,<sup>25</sup> because the substrate membrane contained abundant carboxyl groups after hydrolysis and the prepared nanofiltration membranes were also the same due to the hydrolyzation of unreacted TMC monomers. The absorption peak at 2243  $\text{cm}^{-1}$  was attributed to  $-\text{C}\equiv\text{N}$  in HPAN substrate.<sup>25</sup> The absorption peaks appeared at 1623 and 1385  $\text{cm}^{-1}$  in TFC and TFN membranes were related to  $-\text{C}=\text{O}$  and  $-\text{C}-\text{N}$  in amide groups, respectively,<sup>12,26</sup> which indicated the PA layer was successfully fabricated on HPAN substrate after interfacial polymerization. The absorption peak at 771  $\text{cm}^{-1}$  due to  $\text{Zr}-\text{O}$  could only be observed in TFN membranes,<sup>12</sup> indicating the existence of UiO-66- $\text{NH}_2$ -PC on TFN membrane surfaces.

XPS measurement was used to further characterize the chemical structure of TFN membranes. The XPS survey spectra of TFN-0.10 were shown in Fig. 9. As shown in Fig. 9(a), the chemical elements of TFN-0.10 included carbon, oxygen, nitrogen and zirconium. The high-resolution XPS spectrum of each element was shown in Fig. 9(b-e). The XPS spectrum of C 1s could be resolved into 3 peaks at 287.8, 285.8, and 284.6 eV, which were attributed to  $\text{C}=\text{O}$ ,  $\text{C}-\text{N}$  or  $\text{C}-\text{O}$ , and  $\text{C}-\text{C}$ , respectively.<sup>27,28</sup> The N 1s spectrum could be fitted to two peaks at 399.9 and 399.3 eV which were assigned to  $\text{C}-\text{N}$  in PIP monomer and  $\text{N}-\text{C}=\text{O}$  in polyamide, respectively indicating the polyamide selective layer successfully formed. The O spectrum could be fitted to 3 peaks at 531.7, 531.3, and 530.5 eV, respectively. The peak at 531.7 eV was ascribed to  $\text{C}-\text{O}$  of carboxyl groups from MOF nanoparticles and hydrolyzed acyl chloride groups in TMC. The peak at 531.3 eV was ascribed to  $\text{Zr}-\text{O}$  of MOF nanoparticles, and the peak at 530.5 eV was ascribed to  $\text{C}=\text{O}$  from acylamino, carboxyl groups and MOF nanoparticles in selective layer. The Zr element showed two peaks at 184.7 and 182.3 eV. From Fig. 9(d and e), the existence of Zr element and  $\text{Zr}-\text{O}$  bonds revealed the UiO-66- $\text{NH}_2$ -PC nanoparticles loaded on the membrane surface after interfacial polymerization process.

**3.2.3 XRD patterns of the prepared membranes.** XRD patterns of HPAN substrate and the prepared membranes were

shown in Fig. 10. All the membranes displayed three conspicuous peaks within  $15^\circ$  to  $30^\circ$  which were from HPAN substrate. The two strong characteristic peaks of UiO-66- $\text{NH}_2$ -PC at  $7.3^\circ$  and  $8.4^\circ$  could be observed in TFN membranes, which indicated the successful loading of UiO-66- $\text{NH}_2$ -PC in TFN membranes.

**3.2.4 Hydrophilicity of the prepared membranes.** The influence of UiO-66- $\text{NH}_2$ -PC on the hydrophilicity of TFC and TFN membranes was characterized by water contact angle. As shown in Fig. 11, TFC membrane displayed the lowest contact angle, and with the increase of UiO-66- $\text{NH}_2$ -PC content, the contact angle of TFN membranes presented a slight upward trend, indicating the ascending hydrophobicity of TFN membranes. In order to increase the dispersibility of nanoparticles in organic phase, the surface of nanoparticles needed to hold the character of nonpolarity, low surface energy so as to increase the compatibility with organic solvent owing to the nonpolar intrinsic character of organic phase.<sup>16,29</sup> The modification of UiO-66- $\text{NH}_2$  by palmitoyl chloride could increase the compatibility between UiO-66- $\text{NH}_2$  and cyclohexane due to the existence of nonpolar alkyl which possessed the similar character of hexane, and thus UiO-66- $\text{NH}_2$ -PC could get good dispersibility. But it was for this reason that the hydrophilicity of the modified nanoparticles declined. After loading UiO-66- $\text{NH}_2$ -PC on membrane surface, the hydrophilicity of the membrane surface would also decline, so the water contact angle of TFN membranes increased compared with TFC membrane. But the increment was not significant under UiO-66- $\text{NH}_2$ -PC loading amount within 0.10% w/v. As shown in Fig. 11, the water contact angle was  $41.9 \pm 2.2^\circ$  for TFC membrane and increased to  $46.7 \pm 6.0^\circ$  for TFN-0.10.

**3.2.5 Surface potential of TFC and TFN membranes.** According to the separation mechanism of nanofiltration membranes, the charged membrane surface can interact with ions and solute by electrostatic force so as to exclude opposite electrical substances, which is called the Donnan effect. The surface charge of the prepared membrane was characterized by zeta potential with pH value spanning from 3 to 10 and the results were displayed in Fig. 12. It could be seen that all the membrane showed higher zeta potential at low pH value, and the zeta potential decreased with the pH value increasing. Only at  $\text{pH} = 3$ , the membranes possessed slightly positive charge, which could be ascribed to the protonation of unreacted amino groups in PIP monomer and the protonation of amido bonds in polyamide, because N atoms could combine  $\text{H}^+$  by coordination. When the pH value was larger than 3, the coordination of amino groups and amido bonds would disintegrate to a certain extent leading to the loss of positive charge. And simultaneously, the  $-\text{COOH}$  formed by the hydrolysis of unreacted  $-\text{COCl}$  of TMC monomers gradually deprotonated, which made the membrane surface turn into negatively charged.<sup>30</sup> Under neutral conditions ( $\text{pH} = 7$ ), all the TFC and TFN membranes were negatively charged, which was ascribed to the unreacted  $-\text{COCl}$  of TMC monomers of the polyamide nanofiltration membranes. However, the zeta potential of TFN membranes was higher around neutral conditions with the UiO-66- $\text{NH}_2$ -PC loading amount increasing. This could be explained by the positively charged character of UiO-66- $\text{NH}_2$ -PC nanoparticles



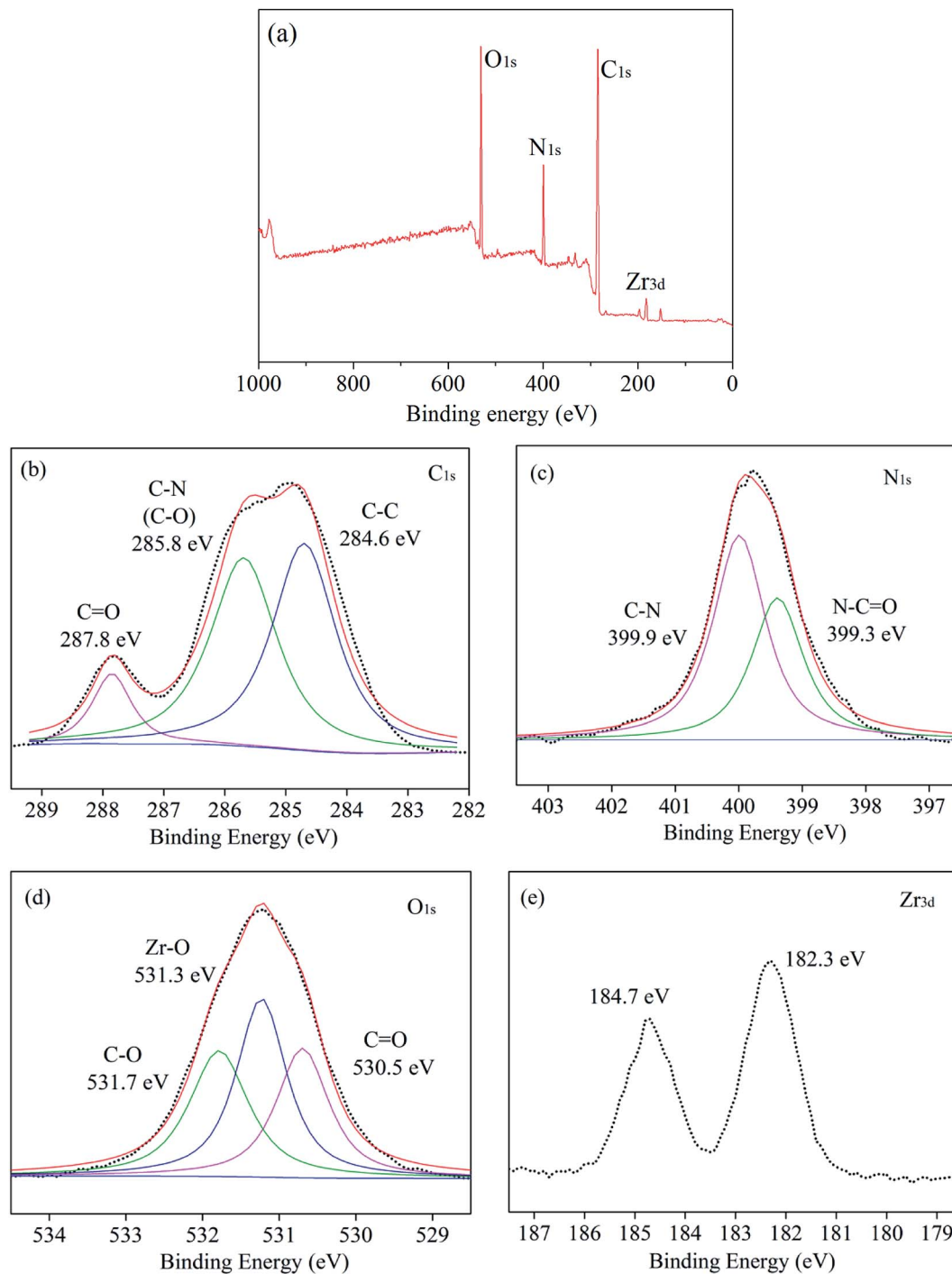


Fig. 9 XPS survey spectra of TFN-0.10 membrane.

due to the existence of amino groups and zirconium ions in the framework structures.<sup>31,32</sup>

**3.2.6 Surface roughness of TFC and TFN membranes.** The surface roughness of TFC and TFN membranes was studied by AFM measurement. The three-dimensional surface topography of the membranes was displayed in Fig. 13. The root average arithmetic roughness ( $R_a$ ) and root mean surface roughness ( $R_q$ ) of the prepared membranes were listed in Table 1.

The surface topography images of the prepared membranes also displayed “ridge and valley” morphologies, which was in accordance with FE-SEM images of the membrane surfaces in Fig. 6. As shown in Table 1, the  $R_a$  and  $R_q$  value increased with the increase of UiO-66-NH<sub>2</sub>-PC loading amount indicating the membranes became rougher after loading nanoparticles on membrane surface. The same phenomena about other nano-materials were also achieved in the previous researches.<sup>33,34</sup> The







Fig. 10 XRD patterns of UiO-66-NH<sub>2</sub>-PC, HPAN substrate and the prepared membranes.

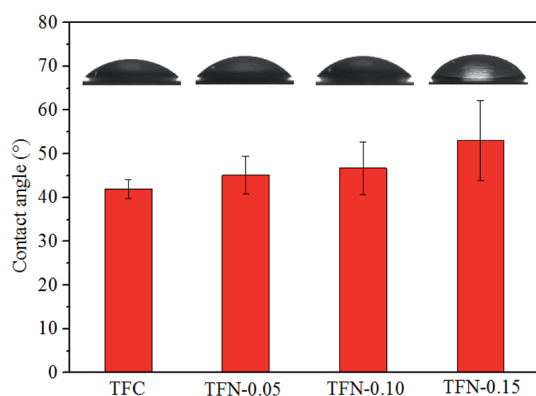


Fig. 11 Contact angle of TFC and TFN membranes.



Fig. 12 Zeta potential of TFC and TFN membranes.

rougher membrane surface could provide larger surface area for mass transfer to obtain a higher permeability.

### 3.3 Nanofiltration performance of the prepared membranes

**3.3.1 Determination of pre-filtration time.** The nanofiltration performance of the prepared TFC and TFN

membranes were tested at 4 bar. Before test, the prepared membrane needed to be wetted in water to dissolve unreacted reagents distributed within the polyamide layer,<sup>35</sup> and also compacted to get a stable separation performance.<sup>36</sup> So the prepared membranes were pre-filtrated at operation pressure of 4 bar for a specific period to determine the needed pre-filtration time. The pre-filtration process was carried out using Na<sub>2</sub>SO<sub>4</sub> solution (0.1% w/v), and the solution flux and Na<sub>2</sub>SO<sub>4</sub> rejection property were shown in Fig. 14. With the filtration time going on, the Na<sub>2</sub>SO<sub>4</sub> rejection increased continuously and the permeation flux decreased continuously. The reason was that, the unreacted monomer reagents within the polyamide macromolecule chains were washed out and the polyamide selective layer became denser under filtration pressure due to compaction and rearrangement of polyamide chains during pre-filtration process, which led to the increase of rejection property and decrease of permeability. When the pre-filtration time reached 50 min the rejection property and permeation flux came up to a nearly stable level. According to the above discussion, the pre-filtration time was set at least 50 min in the following experiments.

**3.3.2 Influence of UiO-66-NH<sub>2</sub>-PC loading amount.** The permeability of the prepared membranes was measured by ultrapure water and the rejection properties were measured by Na<sub>2</sub>SO<sub>4</sub>, MgSO<sub>4</sub>, and NaCl solution. The concentrations of the 3 kinds of typical salt solution were all 0.1% w/v. Before measurement, all the membranes were pre-filtrated for at least 50 min to get a stable performance and the results were shown in Fig. 15.

As displayed in Fig. 15, the pure water permeability (PWP) increased from 8.1 LMH bar<sup>-1</sup> for TFC membrane to 12.4 LMH bar<sup>-1</sup> for TFN-0.15. The increased PWP was largely ascribed to the following factors: firstly, the adding of nanomaterial increased the membrane free volume because the added nanomaterial could interfere with polyamide chain packing;<sup>37</sup> secondly, the intrinsic nanopores of the UiO-66-NH<sub>2</sub>-PC material and the formation of nanomaterial/polyamide interfaces could supply additional passageways for water passing through the membrane.<sup>9</sup> Due to the above reasons, the permeability increased continuously with the increase of UiO-66-NH<sub>2</sub>-PC loading amount.

The rejection properties of the prepared membrane slightly decreased continuously with the increase of UiO-66-NH<sub>2</sub>-PC loading amount. That was ascribed to the formation of the nanomaterial/polyamide interfaces, which led to the leakage of solute passing through the membrane selective layers. The decrease of rejection properties in TFN membranes is a general phenomenon that was reported in other literature.<sup>38–40</sup> It should be noted that all the prepared membranes exhibited the rejection property order of MgSO<sub>4</sub> > Na<sub>2</sub>SO<sub>4</sub> > NaCl, which could be explained by the rejection mechanism of nanofiltration membranes. It was known that the membrane rejection property was based on both size sieving effect and Donnan effect.<sup>41</sup> The hydrated diameters of the salt ions were Mg<sup>2+</sup> (0.86 nm) > Na<sup>+</sup> (0.72 nm), SO<sub>4</sub><sup>2-</sup> (0.76 nm) > Cl<sup>-</sup> (0.66 nm).<sup>42</sup> All the membranes showed negatively zeta potential and thus could repulse the same charged SO<sub>4</sub><sup>2-</sup> and Cl<sup>-</sup>, but the divalent ions



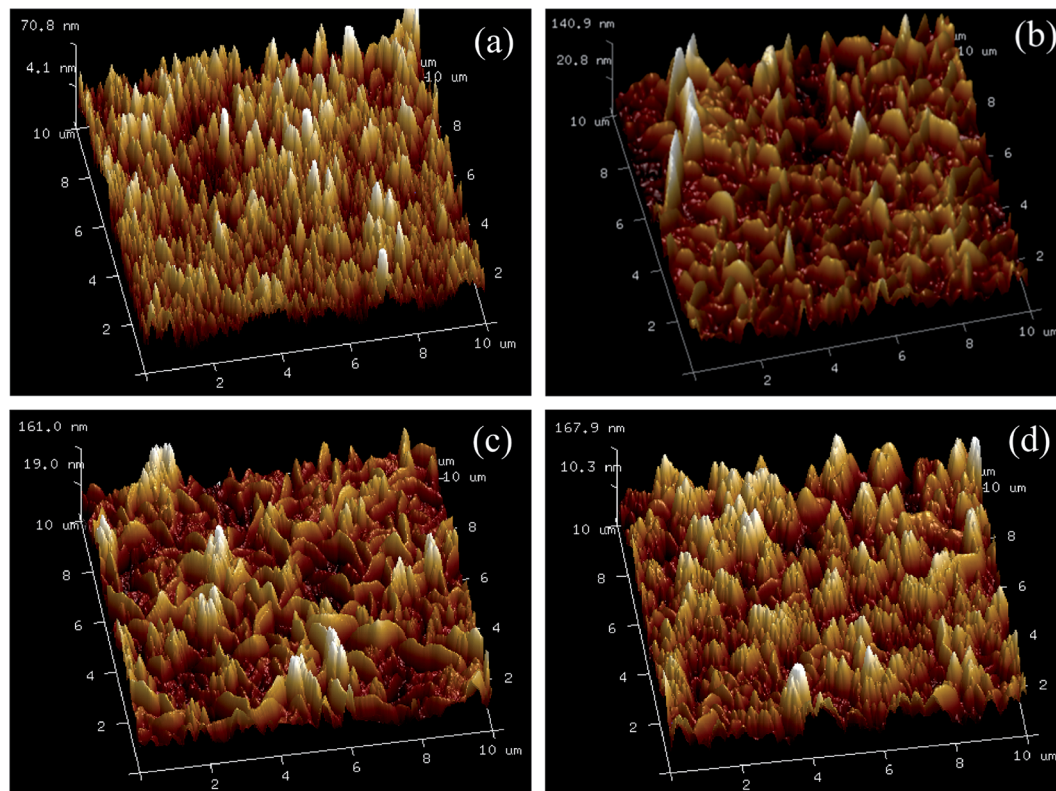


Fig. 13 Three-dimensional surface topography of TFC and TFN membranes.

Table 1 Roughness of the prepared membranes

| Membrane   | TFC  | TFN-0.05 | TFN-0.10 | TFN-0.15 |
|------------|------|----------|----------|----------|
| $R_a$ (nm) | 15.0 | 24.6     | 30.6     | 37.8     |
| $R_q$ (nm) | 19.0 | 32.1     | 39.1     | 46.9     |

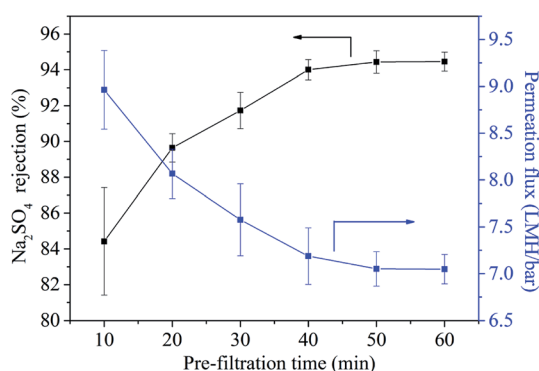


Fig. 14 Influence of pre-filtration time on separation performance.

were easy to be rejected than monovalent ions due to the stronger electronegativity and larger hydrated diameter. So the membranes exhibited higher rejection property of sulfate than chlorate. The rejection of  $MgSO_4 > Na_2SO_4$  was due to the larger hydrated diameter of  $Mg^{2+}$ , which was in accordance with the previous research in other literature.<sup>10</sup>

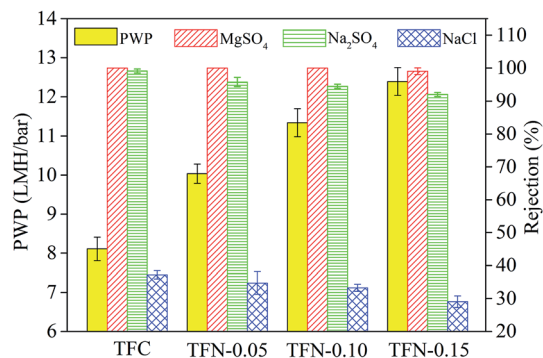


Fig. 15 Influence of UiO-66-NH<sub>2</sub>-PC loading amount on separation performance.

When the UiO-66-NH<sub>2</sub>-PC loading amount was within 0.10% w/v, the  $MgSO_4$  rejection was about 100% and NaCl rejection was above 30%, so the UiO-66-NH<sub>2</sub>-PC loading amount of 0.10% w/v was an acceptable value.

**3.3.3 Influence of operation pressure on TFN membrane property.** The TFN-0.10 was used to study the influence of operation pressure on nanofiltration performance. The nanofiltration experiment was carried out at the operation pressure of 2, 4, 6 and 8 bar using  $Na_2SO_4$  solution with the concentration of 0.1% w/v. The rejection property and solution permeation flux were shown in Fig. 16. As exhibited in the results, the flux rose linearly with the operation pressure increasing. From



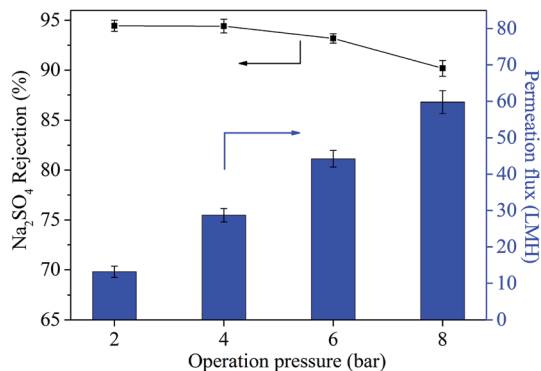


Fig. 16 Influence of operation pressure.

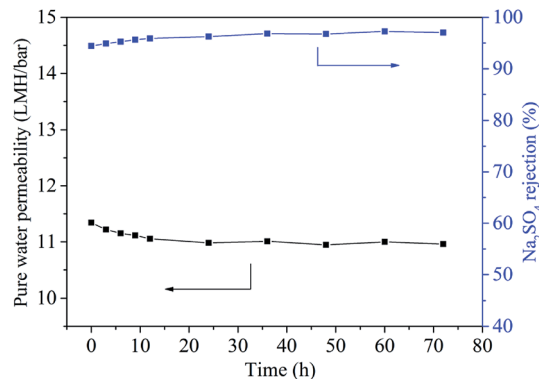


Fig. 18 Long-term stability of TFN-0.10 membrane.

the classical solution diffusion model, the theoretical permeation flux could be given as follows:

$$J_w = A(\Delta p - \Delta \pi)$$

The  $J_w$  represents water flux and  $A$  represents permeability parameter.  $\Delta p$  and  $\Delta \pi$  refer to the operation pressure and osmotic pressure, respectively. It could be found that  $J_w$  was the function of  $\Delta p$  and there was a linear relationship between  $J_w$  and  $\Delta p$ .<sup>43</sup> It was worth noting that the permeation flux at the operation pressure of 4 bar was 28.7 LMH, which was much lower than the pure water permeability of 11.3 LMH bar<sup>-1</sup>. This was attributed to the existence of osmotic pressure ( $\Delta \pi$ ) caused by the concentration polarization between feed side and the permeation side of the membrane.

The operation pressure also influenced the rejection property of TFN-0.10 membrane. With the increase of operation pressure the Na<sub>2</sub>SO<sub>4</sub> rejection decreased continuously, which was in accordance with the reported literature.<sup>15</sup> This phenomenon could be explained by the formation of voids at nanoparticle/polyamide interfaces.<sup>32</sup> Considering the mobility difference between rigid inorganic nanoparticles and flexible organic polyamide matrix, high pressure might tear and weaken the interfacial interaction between nanoparticles and polyamide matrix, because rigid inorganic nanoparticles could not move flexibly and change shape with polyamide chain

synchronously and hence led to the formation of voids at their interfaces.

**3.3.4 Comparison of nanofiltration performance.** As discussed above, the modified nanomaterial could get better dispersibility and hence reduce aggregation in the interfacial polymerization process to prepare high performance nanofiltration membranes. In order to confirm the above conclusion, the TFN membranes prepared with pristine UiO-66-NH<sub>2</sub> and UiO-66 were also measured to compare with that prepared with modified UiO-66-NH<sub>2</sub>-PC and the results were shown in Fig. 17. The TFN membranes prepared with UiO-66-NH<sub>2</sub> and UiO-66 nanomaterials showed higher water permeability but lower rejection properties than that prepared with UiO-66-NH<sub>2</sub>-PC. The results were due to the poor dispersibility of unmodified nanomaterials in organic phase which led to the serious aggregation of nanoparticles on membrane surfaces, which could be seen in Fig. S2.† The results also revealed that UiO-66-NH<sub>2</sub>-PC was more preferable to prepare high rejection TFN membrane due to its better dispersibility in organic phase than UiO-66-NH<sub>2</sub> and UiO-66.

**3.3.5 Long-term stability of TFN-0.10 membrane.** To measure the long-term stability of the prepared TFN membranes, TFN-0.10 membrane was employed to test the membrane property at 4 bar. As shown in Fig. 18, the pure water permeability decreased slightly with the increase of Na<sub>2</sub>SO<sub>4</sub> rejection at early stage due to the compaction and rearrangement of polyamide chains.<sup>44</sup> And then the permeability and rejection property reached a relatively stable level and kept nearly unchanged during the test. The result revealed a stable separation performance of TFN-0.10 membrane. The surface morphology of TFN-0.10 membrane after 72 h filtration was shown in Fig. S3.†

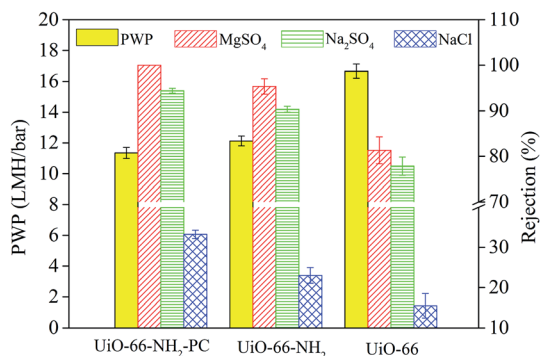


Fig. 17 Nanofiltration performance of TFN membranes prepared with different MOF nanomaterials.

## 4 Conclusion

In this study, the surface modified UiO-66-NH<sub>2</sub> nanoparticles were dispersed in organic phase and introduced into the preparation process of TFN membranes. The surface modification could increase the dispersibility of the synthesized UiO-66-NH<sub>2</sub> nanoparticles and hence reduce the aggregation of nanoparticles in organic phase to prepare high performance





nanofiltration membranes. The prepared TFC and TFN membranes displayed typical “ridge-valley” shaped Turing structure surface morphology. The SEM, ATR-FTIR and XPS characterization demonstrated the polyamide layer was fabricated on HPAN substrates and the modified UiO-66-NH<sub>2</sub> nanoparticles were loaded on the membrane surfaces. Hydrophobicity, surface roughness and zeta potential of TFN membrane increased compared with TFC membrane. The TFN membranes showed higher water permeability and slightly lower rejection properties with the increase of UiO-66-NH<sub>2</sub>-PC concentration in organic phase. Compared with the TFN membranes prepared with pristine UiO-66 and UiO-66-NH<sub>2</sub>, the TFN membrane prepared with modified UiO-66-NH<sub>2</sub> displayed higher salt rejection properties due to the better dispersibility after modification. Furthermore, the membrane performance was stable in the long-term operation test.

## Conflicts of interest

There are no conflicts to declare.

## Acknowledgements

This work was supported by the National Natural Science Foundation of China (No. 21908040 and 21878068), the Natural Science Foundation of Hebei Province (B2017202056), the Program for Top 100 Innovative Talents in Colleges and Universities of Hebei Province (SLRC2017029) and Hebei High Level Personnel of Support Program (A2016002027).

## References

- W. J. Koros and R. P. Lively, Water and beyond: expanding the spectrum of large-scale energy efficient separation processes, *AIChE J.*, 2012, **58**, 2624–2633.
- M. Padaki, R. S. Murali, M. S. Abdullah, N. Misdan, A. Moslehiani, M. A. Kassim, N. Hilal and A. F. Ismail, Membrane technology enhancement in oil–water separation. A review, *Desalination*, 2015, **357**, 197–207.
- C. Castel and E. Favre, Membrane separations and energy efficiency, *J. Membr. Sci.*, 2018, **548**, 345–357.
- A. Ahmad, D. Lokhat, Y. Wang and M. Rafatullah, Recent Advances in Nanofiltration Membrane Techniques for Separation of Toxic Metals from Wastewater, *Nanotechnology for Sustainable Water Resources*, 2018, pp. 477–500.
- H. B. Park, J. Kamcev, L. M. Robeson, M. Elimelech and B. D. Freeman, Maximizing the right stuff: the trade-off between membrane permeability and selectivity, *Science*, 2017, **356**, eaab0530.
- B.-H. Jeong, E. M. Hoek, Y. Yan, A. Subramani, X. Huang, G. Hurwitz, A. K. Ghosh and A. Jawor, Interfacial polymerization of thin film nanocomposites: a new concept for reverse osmosis membranes, *J. Membr. Sci.*, 2007, **294**, 1–7.
- M. Paul and S. D. Jons, Chemistry and fabrication of polymeric nanofiltration membranes: a review, *Poly*, 2016, **103**, 417–456.
- J. L. Rowsell and O. M. Yaghi, Metal–organic frameworks: a new class of porous materials, *Microporous Mesoporous Mater.*, 2004, **73**, 3–14.
- X. Cheng, X. Jiang, Y. Zhang, C. H. Lau, Z. Xie, D. Ng, S. J. Smith, M. R. Hill and L. Shao, Building Additional Passageways in Polyamide Membranes with Hydrostable Metal Organic Frameworks To Recycle and Remove Organic Solutes from Various Solvents, *ACS Appl. Mater. Interfaces*, 2017, **9**, 38877–38886.
- Y. He, Y. P. Tang, D. Ma and T.-S. Chung, UiO-66 incorporated thin-film nanocomposite membranes for efficient selenium and arsenic removal, *J. Membr. Sci.*, 2017, **541**, 262–270.
- G. Lai, W. Lau, S. Gray, T. Matsuura, R. J. Gohari, M. Subramanian, S. Lai, C. Ong, A. Ismail and D. Emazadah, A practical approach to synthesize polyamide thin film nanocomposite (TFN) membranes with improved separation properties for water/wastewater treatment, *J. Mater. Chem. A*, 2016, **4**, 4134–4144.
- M. Golpour and M. Pakizeh, Preparation and characterization of new PA-MOF/PPSU-GO membrane for the separation of KHI from water, *Chem. Eng. J.*, 2018, **345**, 221–232.
- R. Zhang, S. Ji, N. Wang, L. Wang, G. Zhang and J. R. Li, Coordination-driven in situ self-assembly strategy for the preparation of metal–organic framework hybrid membranes, *Angew. Chem., Int. Ed.*, 2014, **53**, 9775–9779.
- N. Wang, T. Liu, H. Shen, S. Ji, J. R. Li and R. Zhang, Ceramic tubular MOF hybrid membrane fabricated through in situ layer-by-layer self-assembly for nanofiltration, *AIChE J.*, 2016, **62**, 538–546.
- J. Zhu, L. Qin, A. Uliana, J. Hou, J. Wang, Y. Zhang, X. Li, S. Yuan, J. Li and M. Tian, Elevated performance of thin film nanocomposite membranes enabled by modified hydrophilic MOFs for nanofiltration, *ACS Appl. Mater. Interfaces*, 2017, **9**, 1975–1986.
- X. Guo, D. Liu, T. Han, H. Huang, Q. Yang and C. Zhong, Preparation of thin film nanocomposite membranes with surface modified MOF for high flux organic solvent nanofiltration, *AIChE J.*, 2017, **63**, 1303–1312.
- A. Schaate, P. Roy, A. Godt, J. Lippke, F. Waltz, M. Wiebecke and P. Behrens, Modulated synthesis of Zr-based metal–organic frameworks: from nano to single crystals, *Chem.–Eur. J.*, 2011, **17**, 6643–6651.
- Z. Hu, Y. Peng, Z. Kang, Y. Qian and D. Zhao, A modulated hydrothermal (MHT) approach for the facile synthesis of UiO-66-type MOFs, *Inorg. Chem.*, 2015, **54**, 4862–4868.
- L. Wan, C. Zhou, K. Xu, B. Feng and A. Huang, Synthesis of highly stable UiO-66-NH<sub>2</sub> membranes with high ions rejection for seawater desalination, *Microporous Mesoporous Mater.*, 2017, **252**, 207–213.
- C. Van Goethem, R. Verbeke, S. Hermans, R. Bernstein and I. Vankelecom, Controlled positioning of MOFs in



- interfacially polymerized thin-film nanocomposites, *J. Mater. Chem. A*, 2016, **4**, 16368–16376.
- 21 H. Wu, B. Tang and P. Wu, Optimizing polyamide thin film composite membrane covalently bonded with modified mesoporous silica nanoparticles, *J. Membr. Sci.*, 2013, **428**, 341–348.
- 22 W. Fang, L. Shi and R. Wang, Mixed polyamide-based composite nanofiltration hollow fiber membranes with improved low-pressure water softening capability, *J. Membr. Sci.*, 2014, **468**, 52–61.
- 23 Z. Tan, S. Chen, X. Peng, L. Zhang and C. Gao, Polyamide membranes with nanoscale Turing structures for water purification, *Science*, 2018, **360**, 518–521.
- 24 Y. Shen, H. Wang, X. Zhang and Y. Zhang, MoS<sub>2</sub> nanosheets functionalized composite mixed matrix membrane for enhanced CO<sub>2</sub> capture via surface drop-coating method, *ACS Appl. Mater. Interfaces*, 2016, **8**, 23371–23378.
- 25 H. Zhang, H. Mao, J. Wang, R. Ding, Z. Du, J. Liu and S. Cao, Mineralization-inspired preparation of composite membranes with polyethyleneimine–nanoparticle hybrid active layer for solvent resistant nanofiltration, *J. Membr. Sci.*, 2014, **470**, 70–79.
- 26 Q.-F. An, W.-D. Sun, Q. Zhao, Y.-L. Ji and C.-J. Gao, Study on a novel nanofiltration membrane prepared by interfacial polymerization with zwitterionic amine monomers, *J. Membr. Sci.*, 2013, **431**, 171–179.
- 27 L. Bai, Y. Liu, N. Bossa, A. Ding, N. Ren, G. Li, H. Liang and M. R. Wiesner, Incorporation of Cellulose Nanocrystals (CNCs) into the Polyamide Layer of Thin-Film Composite (TFC) Nanofiltration Membranes for Enhanced Separation Performance and Antifouling Properties, *Environ. Sci. Technol.*, 2018, **52**, 11178–11187.
- 28 S.-H. Park, Y.-S. Ko, S.-J. Park, J. S. Lee, J. Cho, K.-Y. Baek, I. T. Kim, K. Woo and J.-H. Lee, Immobilization of silver nanoparticle-decorated silica particles on polyamide thin film composite membranes for antibacterial properties, *J. Membr. Sci.*, 2016, **499**, 80–91.
- 29 W. Lau, S. Gray, T. Matsuura, D. Emadzadeh, J. P. Chen and A. Ismail, A review on polyamide thin film nanocomposite (TFN) membranes: history, applications, challenges and approaches, *Water Res.*, 2015, **80**, 306–324.
- 30 F. Yang, S. Zhang, D. Yang and X. Jian, Preparation and characterization of polypiperazine amide/PPESK hollow fiber composite nanofiltration membrane, *J. Membr. Sci.*, 2007, **301**, 85–92.
- 31 S. Wu, Y. Ge, Y. Wang, X. Chen, F. Li, H. Xuan and X. Li, Adsorption of Cr(VI) on nano UiO-66-NH<sub>2</sub> MOFs in water, *Environ. Technol.*, 2018, **39**, 1937–1948.
- 32 H. Liu, J. Gao, G. Liu, M. Zhang and Y. Jiang, Enhancing permeability of thin film nanocomposite (TFN) membranes via covalent linking of polyamide with the incorporated metal–organic frameworks, *Ind. Eng. Chem. Res.*, 2019, **58**, 8772–8783.
- 33 Y. Xu, X. Gao, X. Wang, Q. Wang, Z. Ji, X. Wang, T. Wu and C. Gao, Highly and stably water permeable thin film nanocomposite membranes doped with MIL-101 (Cr) nanoparticles for reverse osmosis application, *Materials*, 2016, **9**, 870.
- 34 H. Wu, B. Tang and P. Wu, Optimization, characterization and nanofiltration properties test of MWNTs/polyester thin film nanocomposite membrane, *J. Membr. Sci.*, 2013, **428**, 425–433.
- 35 S. Yu, M. Liu, Z. Lü, Y. Zhou and C. Gao, Aromatic-cycloaliphatic polyamide thin-film composite membrane with improved chlorine resistance prepared from m-phenylenediamine-4-methyl and cyclohexane-1,3,5-tricarbonyl chloride, *J. Membr. Sci.*, 2009, **344**, 155–164.
- 36 S. Lin, H. Huang, Y. Zeng, L. Zhang and L. a. Hou, Facile surface modification by aldehydes to enhance chlorine resistance of polyamide thin film composite membranes, *J. Membr. Sci.*, 2016, **518**, 40–49.
- 37 S. Bano, A. Mahmood, S.-J. Kim and K.-H. Lee, Graphene oxide modified polyamide nanofiltration membrane with improved flux and antifouling properties, *J. Mater. Chem. A*, 2015, **3**, 2065–2071.
- 38 I. H. Aljundi, Desalination characteristics of TFN-RO membrane incorporated with ZIF-8 nanoparticles, *Desalination*, 2017, **420**, 12–20.
- 39 C. Wang, Z. Li, J. Chen, Z. Li, Y. Yin, L. Cao, Y. Zhong and H. Wu, Covalent organic framework modified polyamide nanofiltration membrane with enhanced performance for desalination, *J. Membr. Sci.*, 2017, **523**, 273–281.
- 40 H. Wu, H. Sun, W. Hong, L. Mao and Y. Liu, Improvement of polyamide thin film nanocomposite membrane assisted by tannic acid–Fe<sup>III</sup> functionalized multiwall carbon nanotubes, *ACS Appl. Mater. Interfaces*, 2017, **9**, 32255–32263.
- 41 C. Hu, Z. Liu, X. Lu, J. Sun, H. Liu and J. Qu, Enhancement of the Donnan effect through capacitive ion increase using an electroconductive rGO-CNT nanofiltration membrane, *J. Mater. Chem. A*, 2018, **6**, 4737–4745.
- 42 X. You, H. Wu, Y. Su, J. Yuan, R. Zhang, Q. Yu, M. Wu, Z. Jiang and X. Cao, Precise nanopore tuning for a high-throughput desalination membrane via co-deposition of dopamine and multifunctional POSS, *J. Mater. Chem. A*, 2018, **6**, 13191–13202.
- 43 S. J. Zaidi, F. Fadhilah, Z. Khan and A. Ismail, Salt and water transport in reverse osmosis thin film composite seawater desalination membranes, *Desalination*, 2015, **368**, 202–213.
- 44 G. Férey and C. Serre, Large breathing effects in three-dimensional porous hybrid matter: facts, analyses, rules and consequences, *Chem. Soc. Rev.*, 2009, **38**, 1380–1399.

